SCIENTIFIC OASIS

Spectrum of Mechanical Engineering and Operational Research

Journal homepage: www.smeor-journal.org
eISSN: 3042-0288

An Application of the Mossakovskii-Jäger Procedure for Solving Plane Strain Adhesive Contact Problems of Power-Law Graded Elastic Solids

Markus Heß [1,*], Paul Leonard Giesa[1]

[1] Department of System Dynamics and Friction Physics, Faculty V – Mechanical Engineering and Transport Systems, Technische Universität Berlin, Berlin, Germany

ARTICLE INFO

Article history:
Received 23 February 2024
Received in revised form 17 April 2024
Accepted 25 May 2024
Available online 31 May 2024

Keywords:
Functionally Graded Materials; Plane Strain Contact; Adhesion; Tangential Loading; Compliance Method; JKR-Adhesion; Power-Law Graded Half-Space.

ABSTRACT

Due to the growing demands on performance in mechanical engineering, an increased number of components are being manufactured from functionally graded materials. The prediction of their contact mechanical behavior usually requires complex numerical investigations, involving the finite element method or semi-analytical methods in combination with Fast Fourier Transformation. In the present work, we develop integral equations for solving plane strain contact problems between power-law graded elastic solids based on an incremental procedure introduced by Mossakovskii and revitalized by Jäger. The deduced formulae are very easy to handle and avoid the complicated solution of common singular integral equations. In this way, closed-form analytical solutions are obtained, which can serve as a qualitative estimation of the contact mechanical behavior of real functionally graded materials. Furthermore, we extend the formulae for solving contact problems with adhesion under both normal and tangential loading. The application of the novel method is exemplified by means of the plane strain adhesive contact between a rigid cylinder and a power-law graded half-space. The corresponding closed-form analytical solutions coincide with the results previously obtained only numerically by other authors.

1. Introduction

Wherever components must withstand extreme mechanical, thermal, or chemical stresses, nowadays they are manufactured from functionally graded materials (FGM). By using FGMs, properties such as Young's modulus, fracture toughness, hardness or ductility can be precisely controlled within one component. Classic applications in mechanical engineering include turbine blades and disks, cylinder liners, bearings, cutting tools or piezo-electric ultrasonic transducers. FGMs are also of great significance for other sciences like biology, optoelectronics, or medicine [1]. One modern application from the latter field are orthopedic implants for shoulder, hip, or knee joint replacements. In many cases, functionally graded scaffolds with spatially varying porosity are used

* *Corresponding author.*
E-mail address: markus.hess@tu-berlin.de

https://doi.org/10.31181/smeor1120245

for bone and dental implant applications to mimic the spatial differences in biological and mechanical properties [2,3].

The solution of contact problems is already a major task for homogeneous elastic materials, especially when dissimilar materials are present and arbitrary loading scenarios or effects such as molecular adhesion and lubrication must be considered. The inclusion of functionally graded materials further increases the level of difficulty. In most cases, numerical methods are required. One option are user-friendly FEM-packages, that even allow including some multi-physical interactions between the contacting surfaces. However, unexpected results can emerge whose correctness needs to be questioned and clarified. In such cases and for qualitative prediction of the contact mechanical behavior, analytical treatments under appropriate simplifying assumptions can be extremely useful. Typical methods for finding analytical solutions are summarized in the classical textbooks on contact mechanics [4-6]. A common method is based on the half-space solutions due to line or point forces, which serve as Green's functions, to provide integral equations for the case of distributed normal and tangential tractions transmitted at contact interfaces. For plane contacts, this leads to singular integrals that are sometimes difficult to calculate. As a demonstration let us look at the corresponding equations for a plane contact between two elastically graded solids. Both are assumed as half-planes whose Young's moduli change perpendicular to their surfaces according to the power-law

$$E(y) = E_0\left(\frac{y}{y_0}\right)^k, \; -1 < k < 1, \tag{1}$$

where y_0 denotes the characteristic depth at which the Young's moduli are equal to E_0, irrespective of the exponent k. For negative exponents k, the power-law describes a material whose Young's modulus gradually decreases with depth, starting from a very stiff surface. For positive ones, the elasticity changes from a soft surface to a very stiff core. Fig. 1 illustrates the behavior of Young's modulus with depth for k = ±0.5, two representative exponents which will be used in almost all further analyses.

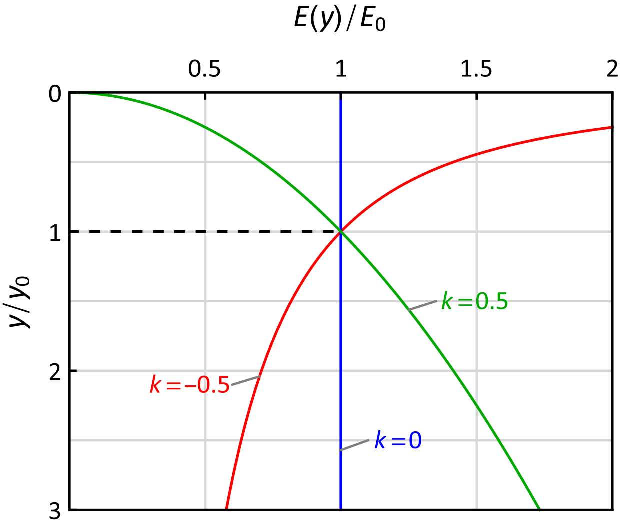

Fig. 1. Variation of Young's modulus towards the interior of a power-law graded half-plane for three representative exponents of elastic inhomogeneity

As mentioned above, we now list the singular integral equations that consider the effect of distributed pressure $p(x)$ and tangential tractions $q(x)$ on the surface displacements of a power-law graded (PLG) half-plane. They were probably first noted in completeness by Popov [7] and read:

$$\begin{aligned} u_x(x) &= \frac{y_0^k g(k,\nu)}{E_0}\int_{-\infty}^{\infty}\frac{q(\xi)\mathrm{d}\xi}{|x-\xi|^k} - \frac{y_0^k l(k,\nu)}{E_0}\int_{-\infty}^{\infty}\frac{p(\xi)\operatorname{sgn}(x-\xi)\mathrm{d}\xi}{|x-\xi|^k}, \\ u_y(x) &= \frac{y_0^k l(k,\nu)}{E_0}\int_{-\infty}^{\infty}\frac{q(\xi)\operatorname{sgn}(x-\xi)\mathrm{d}\xi}{|x-\xi|^k} + \frac{y_0^k b(k,\nu)}{E_0}\int_{-\infty}^{\infty}\frac{p(\xi)\mathrm{d}\xi}{|x-\xi|^k} \end{aligned} \tag{2}$$

with elastic parameters defined by

$$\begin{aligned} g(k,\nu) &:= \frac{1-\nu^2}{k}\sin\left(\frac{\beta(k,\nu)\pi}{2}\right)\frac{k+1}{\beta(k,\nu)}C(k,\nu) =: \left(\frac{k+1}{\beta(k,\nu)}\right)^2 b(k,\nu), \\ l(k,\nu) &:= -\frac{1-\nu^2}{k}\cos\left(\frac{\beta(k,\nu)\pi}{2}\right)C(k,\nu) \end{aligned} \tag{3}$$

and

$$\beta(k,\nu) = \sqrt{\left(1-\frac{k\nu}{1-\nu}\right)(1+k)},\ C(k,\nu) = \frac{2^{k+1}}{\pi}\frac{\Gamma\left(\frac{3+k+\beta(k,\nu)}{2}\right)\Gamma\left(\frac{3+k-\beta(k,\nu)}{2}\right)}{\Gamma(2+k)}. \tag{4}$$

In addition to the contact between a rigid body and a power-law graded solid, we investigate the contact of two power-law graded solids, but for the sake of simplicity the same exponents of elastic inhomogeneity (and characteristic depths) are presumed. A schematic representation of two contacting power-law graded elastic solids with positive in-depth gradings is shown in Fig. 2 on the left (a) whereas the solids on the right (b) consist of negative in-depth gradings, representing a stiff interface and soft cores.

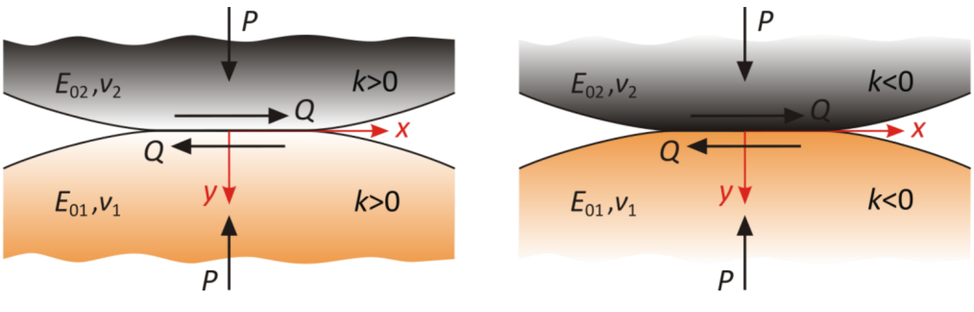

Fig. 2. Schematic representation of the contact between two power-law graded elastic solids: (a) Elastic modulus of both increases with distance from their surfaces, representing a soft interface and stiff cores (b) Elastic modulus of both decreases towards their interior, representing a stiff interface and soft cores

Eqs. (2) also hold for this case, however, the displacements are then to be understood as relative displacements and the elastic parameters must be replaced as follows

$$\frac{g(k,\nu)}{E_0} \to \frac{g(k,\nu_1)}{E_{01}} + \frac{g(k,\nu_2)}{E_{02}}, \frac{l(k,\nu)}{E_0} \to \frac{l(k,\nu_1)}{E_{01}} - \frac{l(k,\nu_2)}{E_{02}}, \frac{b(k,\nu)}{E_0} \to \frac{b(k,\nu_1)}{E_{01}} + \frac{b(k,\nu_2)}{E_{02}}. \tag{5}$$

As expected, the Eqs. (2) are completely decoupled for frictionless contact. However, normal and tangential effects are decoupled as well, if the condition

$$\frac{l(k,\nu_1)}{E_{01}}=\frac{l(k,\nu_2)}{E_{02}} \tag{6}$$

is satisfied. As a result, the Eqs. (2) simplify to

$$\begin{aligned} u_x(x)&=y_0^k\left(\frac{g_1}{E_{01}}+\frac{g_2}{E_{02}}\right)\int_{-\infty}^{\infty}\frac{q(\xi)\mathrm{d}\xi}{|x-\xi|^k} \\ u_y(x)&=y_0^k\left(\frac{b_1}{E_{01}}+\frac{b_2}{E_{02}}\right)\int_{-\infty}^{\infty}\frac{p(\xi)\mathrm{d}\xi}{|x-\xi|^k}\end{aligned}, \tag{7}$$

with $g_i = g(k,\nu_i)$ and $b_i = b(k,\nu_i)$.

The reason why we only treat graded materials according to the power law (1) and additionally assume elastically similarity, i.e. fulfill the condition (6), is that it is one of the few cases that allows closed-form analytical solutions. Even for two power-law graded solids with different exponents of elastic inhomogeneity, the solution of plane contact problems becomes considerably more complicated. Recently, Antipov and Mkhitaryan [8] have proposed a novel solution method based on Gegenbauer orthogonal polynomials, which leads to an infinite system of linear algebraic equations with a special structure that needs to be solved numerically. For in-depth gradings deviating from the power law, analytical solutions become even more complex and are usually only possible in an asymptotic way [9].

As simple as the integral Eqs. (2) and (7) may look, their inversion, when for example knowing the surface displacements within the contact area of a pure normal contact, is mathematically complicated. For the normal contact of a rigid punch and a PLG-solid under non-slipping boundary conditions taking coupling effects into account, Popov [7] solved the weakly singular integral equations in a general form based on a series of Jacobi polynomials. Explicit solutions were given for the pressure and tangential tractions under a flat punch.

In this paper we use a mathematically much simpler method proposed by Mossakovskii [10] and revitalized by Jäger [11]. According to this method, the general solution of a normal contact problem can be constructed from the superposition of incremental flat punch solutions, regardless of whether a symmetrical or asymmetrical contact is present. This also applies to the determination of the stresses within the half-plane, which can be determined through a superposition of corresponding incremental Muskhelishvili potentials [12,13]. Tangential or torsional contacts can be solved in a similar way. In a recent paper [14], the method was applied for solving plane non-slipping normal contacts of dissimilar but elastically homogeneous materials and integral equations for the case with finite friction under the simplifying Goodman assumption were given as well. A general solution for axisymmetric normal contacts of power-law graded elastic solids based on the Mossakovskii-Jäger procedure has been derived by Jin and Guo [15] and for arbitrary normal and tangential loading by Heß and Li [16]. We will adopt this procedure for the treatment of plane contacts.

The paper is structured as follows. In Sect. 2, general formulae for the non-adhesive plane strain normal contact of power-law graded solids are derived based on the incremental method. In Sect. 3, these formulae are extended to include JKR-adhesion by applying the compliance method. How to consider the influence of an additional tangential line load is illustrated in Sect. 4.3. For the adhesive plane strain contact of a rigid cylinder and a power-law graded half-space, closed-form analytical solutions are derived in Sect. 4. The solutions agree with the results obtained so far only numerically by other authors.

2. Mossakovskii-Jäger Procedure Applied to Plane Normal Contact Problems of PLG-Solids

2.1 Indentation of a Power-Law Graded Elastic Half-Plane by a Flat-Ended Rigid Punch

The method of Mossakovskii and Jäger for deriving general integral solutions for normal contact problems (without friction) demands knowledge of the flat punch solutions. The corresponding contact is shown in Fig. 3 for the case of a rigid flat punch of half-width a and a power-law graded half-plane with positive in-depth grading. Since the normal surface displacement of the half-plane are not bounded at infinity for negative exponents of elastic inhomogeneity, we additionally specify the uniquely defined position $h_y(x)$ of the deformed surface measured from the lowest point of the indentation. Remember that the same problem occurs with elastically homogeneous half-planes, as the displacements are logarithmically divergent. P specifies the normal line load and δ_y the indentation depth (uniquely defined only for positive k).

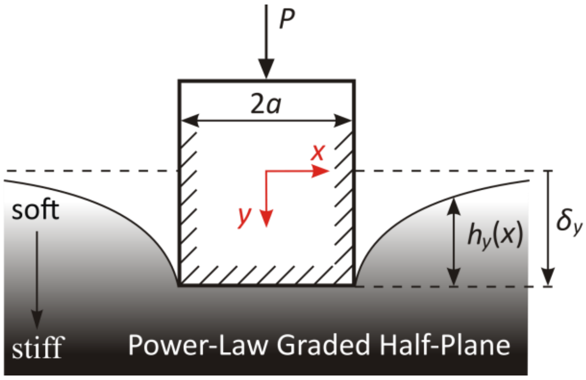

Fig. 3. Indentation of a power-law graded elastic half-plane by a flat rigid punch of half-width *a*

The pressure distribution for frictionless contact already emerged as a special case from Popov's work [7]. However, complete solutions including the surface displacements (for positive k), have been presented by Booker *et al.* [17]. We adopt and extend these solutions:

$$p(x,P)=\frac{\Gamma\left(\frac{2+k}{2}\right)P}{\sqrt{\pi}\,\Gamma\left(\frac{1+k}{2}\right)a}\left(1-\frac{x^2}{a^2}\right)^{\frac{k-1}{2}}, \tag{8}$$

$$h_y(x,P)=\frac{by_0^kP}{E_0a^k}\left[\frac{\Gamma\left(\frac{2+k}{2}\right)\Gamma\left(\frac{1-k}{2}\right)}{\sqrt{\pi}}-\left|\frac{a}{x}\right|^k {}_2\mathrm{F}_1\left(\frac{k}{2},\frac{1+k}{2};\frac{2+k}{2};\frac{a^2}{x^2}\right)\right] \quad \text{for } |x|>a, \tag{9}$$

$$u_y(x,P)=\frac{by_0^kP}{E_0a^k}\begin{cases}\dfrac{\Gamma\left(\frac{2+k}{2}\right)\Gamma\left(\frac{1-k}{2}\right)}{\sqrt{\pi}} & \text{for } |x|\le a\\ \left|\dfrac{a}{x}\right|^k {}_2\mathrm{F}_1\left(\dfrac{k}{2},\dfrac{1+k}{2};\dfrac{2+k}{2};\dfrac{a^2}{x^2}\right) & \text{for } |x|\ge a\end{cases}, \quad 0<k<1, \tag{10}$$

with the hypergeometric function defined by

$${}_2\mathrm{F}_1(a,b;c;z):=\sum_{n=0}^{\infty}\frac{(a)_n(b)_n}{(c)_n}\frac{z^n}{n!},\quad (x)_n:=\frac{\Gamma(x+n)}{\Gamma(x)}, \tag{11}$$

and the Gamma function Γ.

2.2 General Solution by Superposition of Incremental Flat-Punch Solutions

Let us now assume that the power-law graded half-plane is indented by a convex symmetrical punch. The initial state where both bodies are just touching at one point before loading, is depicted in Fig. 4. The shape of the indenter and thus the initial gap is given by the function *f*(*x*). The approximated shape of the indenter in Fig. 4 already indicates that the indentation process can be understood as a sequence of incremental indentations of flat punches with different contact half-widths $0 \le \tilde{a} \le a$.

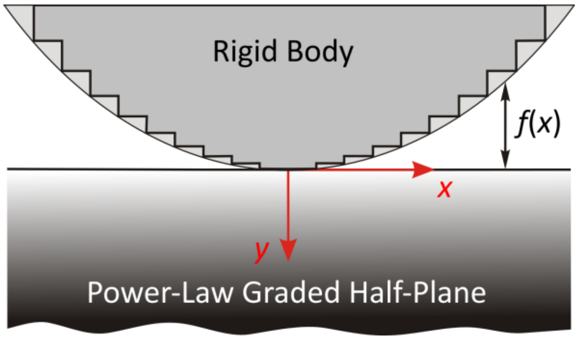

Fig. 4. Indention by a curved rigid punch can be considered as a series of incremental flat-punch indentations of different contact half-widths; *f*(*x*) represents the initial gap function

For this reason, the complete solution of the contact problem can be constructed by an appropriate superposition of incremental flat punch solutions corresponding to different contact half-widths. The incremental contributions of a flat-ended punch of half-width $\tilde{a}$ to pressure and deformations resulting from Eqs. (8) to (10) are

$$\mathrm{d}p\left(x,\tilde{a}\right)=\frac{\Gamma\left(\frac{2+k}{2}\right)P'\left(\tilde{a}\right)\mathrm{d}\tilde{a}}{\sqrt{\pi}\,\Gamma\left(\frac{1+k}{2}\right)\tilde{a}^k\left(\tilde{a}^2-x^2\right)^{\frac{1-k}{2}}}, \tag{12}$$

$$\mathrm{d}h_y\left(x,\tilde{a}\right)=\frac{by_0^kP'\left(\tilde{a}\right)}{E_0\tilde{a}^k}\left[\frac{\Gamma\left(\frac{2+k}{2}\right)\Gamma\left(\frac{1-k}{2}\right)}{\sqrt{\pi}}-\left|\frac{\tilde{a}}{x}\right|^k{}_2\mathrm{F}_1\left(\frac{k}{2},\frac{1+k}{2};\frac{2+k}{2};\frac{\tilde{a}^2}{x^2}\right)\right]\mathrm{d}\tilde{a}\ \text{ for } |x|>\tilde{a}, \tag{13}$$

$$\mathrm{d}u_y\left(x,\tilde{a}\right)=\frac{by_0^kP'\left(\tilde{a}\right)}{E_0\tilde{a}^k}\begin{cases}\dfrac{\Gamma\left(\frac{2+k}{2}\right)\Gamma\left(\frac{1-k}{2}\right)}{\sqrt{\pi}}\mathrm{d}\tilde{a} & \text{for } |x|\le\tilde{a}\\ \left|\dfrac{\tilde{a}}{x}\right|^k{}_2\mathrm{F}_1\left(\dfrac{k}{2},\dfrac{1+k}{2};\dfrac{2+k}{2};\dfrac{\tilde{a}^2}{x^2}\right)\mathrm{d}\tilde{a} & \text{for } |x|\ge\tilde{a}\end{cases},\quad 0<k<1. \tag{14}$$

Only that flat punch solutions corresponding to half-widths $|x| \le \tilde{a} \le a$ contribute to the pressure at a point *x* within the contact region. The sum of these contributions provides

$$p\left(x,a\right)=\frac{\Gamma\left(\frac{2+k}{2}\right)}{\sqrt{\pi}\,\Gamma\left(\frac{1+k}{2}\right)}\int_{|x|}^{a}\frac{n_y\left(\tilde{a}\right)}{\sqrt{\left(\tilde{a}^2-x^2\right)^{1-k}}}\mathrm{d}\tilde{a}, \tag{15}$$

where we have introduced the function

$$n_y\left(\tilde{a}\right):=P'\left(\tilde{a}\right)/\tilde{a}^k. \tag{16}$$

To determine the position $h_y(x)$ of the deformed surface measured from the lowest point of indentation, solutions according to Eq. (13) for different contact half-widths must be added. A distinction between two different cases is necessary. While for points outside the contact region all flat-punch solutions associated with contact half-widths $0 \le \tilde{a} \le a$ must be taken into account, for points x within the contact region only those provide non-zero contributions that belong to smaller half-widths $0 \le \tilde{a} \le |x|$, hence,

$$h_y(x,a) = \frac{b y_0^k}{E_0} \int_0^{\mathrm{Min}\{|x|,a\}} n_y(\tilde{a}) \left[\frac{\Gamma\left(\frac{2+k}{2}\right)\Gamma\left(\frac{1-k}{2}\right)}{\sqrt{\pi}} - \left|\frac{\tilde{a}}{x}\right|^k {}_2\mathrm{F}_1\left(\frac{k}{2}, \frac{1+k}{2}; \frac{2+k}{2}; \frac{\tilde{a}^2}{x^2}\right) \right] \mathrm{d}\tilde{a} . \tag{17}$$

In an analogous way, a governing integral for determining the surface displacement (provided that $0 < k < 1$) can be established:

$$u_y(x,a) = \frac{b y_0^k}{E_0} \left[\int_0^{\mathrm{Min}\{|x|,a\}} n_y(\tilde{a}) \frac{\tilde{a}^k}{|x|^k} {}_2\mathrm{F}_1\left(\frac{k}{2}, \frac{1+k}{2}; \frac{2+k}{2}; \frac{\tilde{a}^2}{x^2}\right) \mathrm{d}\tilde{a} + \frac{\Gamma\left(\frac{2+k}{2}\right)\Gamma\left(\frac{1-k}{2}\right)}{\sqrt{\pi}} \int_{\mathrm{Min}\{|x|,a\}}^{a} n_y(\tilde{a}) \mathrm{d}\tilde{a} \right] . \tag{18}$$

As a special case, from Eq. (18) the indentation depth δ_y emerges as well

$$\delta_y(a) = \frac{b y_0^k}{E_0} \frac{\Gamma\left(\frac{2+k}{2}\right)\Gamma\left(\frac{1-k}{2}\right)}{\sqrt{\pi}} \int_0^a n_y(\tilde{a}) \mathrm{d}\tilde{a}, \quad 0 < k < 1 . \tag{19}$$

Furthermore, the normal line load P as a function of the contact half-width a is obtained by means of Eq. (16)

$$P(a) = \int_0^a n_y(\tilde{a}) \tilde{a}^k \mathrm{d}\tilde{a} . \tag{20}$$

All the above formulae include one and the same function $n_y(\tilde{a})$, which must be determined from the given boundary conditions. We would like to distinguish between two types in the following sections.

2.2.1 Frictionless normal indentation (prescribed normal displacement)

Let us first consider a frictionless normal indentation of a curved rigid punch whose shape is specified by a symmetric function $f(x)$. Obviously, within the contact zone, the position of the half-plane surface measured from the lowest point of the indenter must correspond to the shape of the intender, i.e.

$$h_y(x,a) = f(x), \text{ for } |x| \le a . \tag{21}$$

Substituting Eq. (17) into Eq. (21) and then differentiating both sides by x gives

$$\frac{b k y_0^k}{E_0} \int_0^{|x|} \frac{n_y(\tilde{a}) \tilde{a}^k \,\mathrm{sgn}(x)}{\sqrt{\left(x^2 - \tilde{a}^2\right)^{1+k}}} \mathrm{d}\tilde{a} = f'(x) . \tag{22}$$

Eq. (22) describes a generalized Abel transform whose inversion yields

$$n_y(\tilde{a}) = \frac{2E_0 \cos\left(\frac{k\pi}{2}\right)}{\pi b k y_0^k \tilde{a}^k} \frac{\mathrm{d}}{\mathrm{d}\tilde{a}} \int_0^{\tilde{a}} \frac{x f'(x)}{\sqrt{\left(\tilde{a}^2 - x^2\right)^{1-k}}} \mathrm{d}x \, . \tag{23}$$

2.2.2 Prescribed (symmetric) pressure applied to a surface region of half-width a

Let us now assume that a symmetric pressure distribution is prescribed over a region of width $2a$ on a power-law graded elastic half-plane. This type of boundary condition can be of interest, for example, for the investigation of contacts with adhesion or for the calculation of the final shape of a worn contact subjected to oscillatory shear [18-20]. In this case, the function $n_y(\tilde{a})$ must be determined from Eq. (15). This in turn requires an Abel reverse transform, which leads to

$$n_y(\tilde{a}) = -\frac{2\sqrt{\pi}}{\Gamma\left(\frac{2+k}{2}\right)\Gamma\left(\frac{1-k}{2}\right)} \frac{\mathrm{d}}{\mathrm{d}\tilde{a}} \int_{\tilde{a}}^{a} \frac{|x| p(x)}{\sqrt{\left(x^2 - \tilde{a}^2\right)^{1+k}}} \mathrm{d}x \, . \tag{24}$$

3. General Solution for Normal Contact Problems with JKR-Adhesion

In the following, we establish the governing equations for the solution of the normal contact with adhesion under the classical assumption that adhesive interactions only play a role within the contact region. For the contact between an elastically homogeneous sphere and a rigid, smooth plane, Johnson, Kendall and Roberts (JKR) provided a solution by finding the minimum of the total potential energy. A generalized version of the JKR-theory for application to other geometries and inhomogeneous (but linear) materials was developed by Shull *et al.* [21,22]. We apply this so-called “compliance method” to plane adhesive contacts between PLG-solids.

In the equilibrium of the adhesive contact, the elastic energy release rate G is equal to the work of adhesion $\Delta\gamma$

$$G = \Delta\gamma \, . \tag{25}$$

In the framework of the compliance method the elastic energy release rate can be determined by

$$G = \frac{\left(P_{\text{n.a.}} - P\right)^2}{4S^2} \frac{\mathrm{d}S_y}{\mathrm{d}a}, \quad S_y := \frac{\mathrm{d}P_{\text{n.a.}}}{\mathrm{d}\delta_{y,\text{n.a.}}}, \tag{26}$$

where the index "n.a." denotes the corresponding non-adhesive solution and S_y the normal contact stiffness (which is strictly speaking uniquely defined only for $0<k<1$). The latter can be obtained most easily from Eq. (10) of the non-adhesive flat-punch indentation, as the half-width is fixed here. After substituting into Eq. (26) and application of the equilibrium condition Eq. (25), we obtain

$$P(a) = P_{\text{n.a.}}(a) - \sqrt{\frac{4\Delta\gamma\sqrt{\pi}E_0 a^{k+1}}{b k y_0^k \Gamma\left(\frac{2+k}{2}\right)\Gamma\left(\frac{1-k}{2}\right)}} \, . \tag{27}$$

Hence, the JKR-adhesive contact can be regarded as a superposition of a non-adhesive indentation with a rigid-body translation at fixed contact width. The second term on the right-hand side in Eq. (27) indicates this (unloading) part, which is equivalent to a negative indentation by a rigid flat punch. The pressure distribution and the variables of half-plane deformation are composed in the same way by the corresponding non-adhesive solutions and the flat punch solutions. By using Eqs. (8) to (10) and taking the corresponding “flat punch” line load of Eq. (27) into account, the following results are obtained

$$p(x,a)=p_{\text{n.a.}}(x,a)-\sqrt{\frac{4\Gamma\left(\frac{2+k}{2}\right)\Delta\gamma E_0 a^{k-1}}{\sqrt{\pi}bky_0^k\Gamma\left(\frac{1+k}{2}\right)^2\Gamma\left(\frac{1-k}{2}\right)}}\left(1-\frac{x^2}{a^2}\right)^{\frac{k-1}{2}}, \tag{28}$$

$$h_y(x,a)=h_{y,\text{n.a.}}(x,a)-\sqrt{\frac{4by_0^k\Delta\gamma\sqrt{\pi}a^{1-k}}{E_0k\Gamma\left(\frac{2+k}{2}\right)\Gamma\left(\frac{1-k}{2}\right)}}\left[\frac{\Gamma\left(\frac{2+k}{2}\right)\Gamma\left(\frac{1-k}{2}\right)}{\sqrt{\pi}}-\left|\frac{a}{x}\right|^k {}_2F_1\left(\frac{k}{2},\frac{1+k}{2};\frac{2+k}{2};\frac{a^2}{x^2}\right)\right], \tag{29}$$

$$\delta_y(a)=\delta_{y,\text{n.a.}}(a)-\sqrt{\frac{4\Gamma\left(\frac{2+k}{2}\right)\Gamma\left(\frac{1-k}{2}\right)\Delta\gamma by_0^k a^{1-k}}{\sqrt{\pi}kE_0}},\quad 0<k<1. \tag{30}$$

It is worth noting that Eq. (29) specifies the position of the deformed surface measured from the lowest point of the indentation only for $|x|>a$. For points within the contact zone, it is given by the initial gap function according to the boundary condition (21).

The critical configuration characterized by the half-width a_c, at which the contact loses its stability and detaches, is determined from the condition

$$\left.\frac{\mathrm{d}P(a)}{\mathrm{d}a}\right|_{a=a_c}=0 \Leftrightarrow \left.\frac{\mathrm{d}P_{\text{n.a.}}(a)}{\mathrm{d}a}\right|_{a=a_c}=\frac{k+1}{2}\sqrt{\frac{4\Delta\gamma\sqrt{\pi}E_0a_c^{k-1}}{bky_0^k\Gamma\left(\frac{2+k}{2}\right)\Gamma\left(\frac{1-k}{2}\right)}}. \tag{31}$$

The line load in the critical state P_c (also called adhesion force per unit length) results after substituting the critical half-width in Eq. (27).

Note, that an extension of the compliance method for taking tangential loading into account is presented in Sect. 4.3.

4. Example: Adhesive Contact between a Rigid Cylinder and a Power-Law Graded Half-Plane

To illustrate the simplicity of the solution method, we deal below with the indentation of a PLG-half-plane by a rigid cylinder of radius R. First, the frictionless normal contact without adhesion is solved and then this solution is extended by the corresponding rigid body translation resulting in the solution of the adhesive contact.

4.1 Non-Adhesive Solution

Fig. 5 shows the plane strain indentation of a power-law graded half-space by a parabolic cylinder with radius of curvature R.

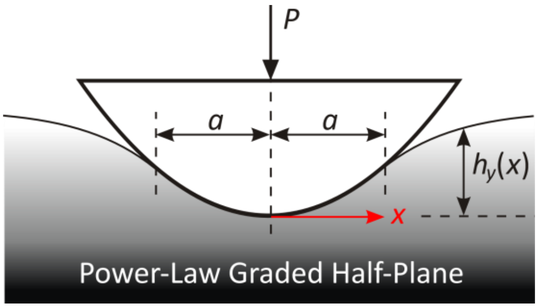

Fig. 5 Plane strain indentation of a power-law graded half-space by a parabolic cylinder with radius of curvature R

The shape of the indenter and thus the initial gap function including its derivative are given by

$$f(x)=\frac{x^2}{2R} \quad \Rightarrow \quad f'(x)=\frac{x}{R}. \tag{32}$$

Substituting this contact profile into Eq. (23) and performing the integral yields

$$n_y(\tilde{a})=\frac{\sqrt{\pi}E_0}{b(k,\nu)k\,y_0^k\,\Gamma\left(\frac{2+k}{2}\right)\Gamma\left(\frac{1-k}{2}\right)}\frac{\tilde{a}}{R}. \tag{33}$$

All defined quantities that characterize the contact were defined exclusively by the above function. The line load P as a function of the contact half-width a follows from Eq. (20) after elementary calculation

$$P(a)=\frac{\sqrt{\pi}E_0 a^{k+2}}{2b(k,\nu)Ry_0^k k\Gamma\left(\frac{4+k}{2}\right)\Gamma\left(\frac{1-k}{2}\right)}. \tag{34}$$

In the limiting case $k\rightarrow 0$, the well-known result of the plane strain Hertzian contact is recovered,

$$P(a_0)=\frac{\pi}{4}\frac{E_0 a_0^2}{\left(1-\nu^2\right)R}, \tag{35}$$

with the corresponding half-width denoted by a_0. If the same line load P is applied, the ratio of the contact half-widths is

$$\frac{a}{a_0}=\left(\frac{\sqrt{\pi}kb(k,\nu)\Gamma\left(\frac{4+k}{2}\right)\Gamma\left(\frac{1-k}{2}\right)}{2\left(1-\nu^2\right)}\right)^{\frac{1}{2+k}}\left(\frac{y_0}{a_0}\right)^{\frac{k}{2+k}}. \tag{36}$$

This ratio is visualized in Fig. 6 as a function of the exponent of the elastic inhomogeneity for three selected characteristic depths and a Poisson's ratio of $\nu = 0.3$. Obviously, the characteristic depth influences the curve significantly. For the two larger characteristic depths $y_0/a_0 = 1$ and $y_0/a_0 = 10$, monotonically increasing curves result, whereby the contact half-widths for negative exponents of elastic inhomogeneity are smaller and for positive exponents larger than the contact half-width for elastically homogeneous material. For the characteristic depth $y_0/a_0=0.1$, however, the contact half-width for negative exponents is greater than for elastically homogeneous material and decreases monotonically. This decrease extends into the range of positive exponents where it reaches a minimum and then increases again.

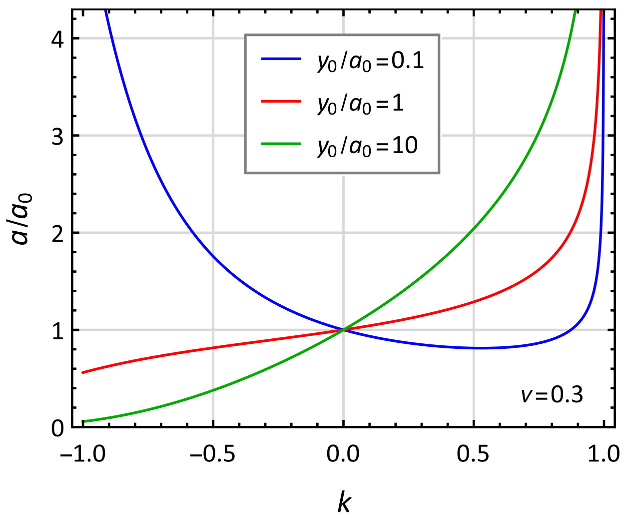

Fig. 6 Normalized contact half-width as a function of the exponent of elastic inhomogeneity k for selected characteristic depths and a Poisson's ratio of $v=0.3$

To determine the pressure distribution, Eq. (33) is used in formula (15). Taking Eq. (34) into account, we obtain

$$p(x,a)=\frac{\Gamma\left(\frac{4+k}{2}\right)P(a)}{\sqrt{\pi}\,\Gamma\left(\frac{3+k}{2}\right)a}\left(1-\frac{x^2}{a^2}\right)^{\frac{1+k}{2}}. \tag{37}$$

The pressure distribution normalized to the mean pressure that occurs when a homogeneous half-plane is indented by the same line load P, is depicted in Fig. 7 for selected values of the exponent of elastic inhomogeneity. Since $y_0=a_0$ was chosen for the characteristic depth, negative exponents result in a smaller contact half-width combined with a larger maximum pressure compared to the elastically homogeneous case. For positive exponents, the opposite behavior arises. As discussed above regarding the contact half-width, the pressure distribution is also significantly influenced by the choice of the characteristic depth, which can sometimes result in completely contrary behavior.

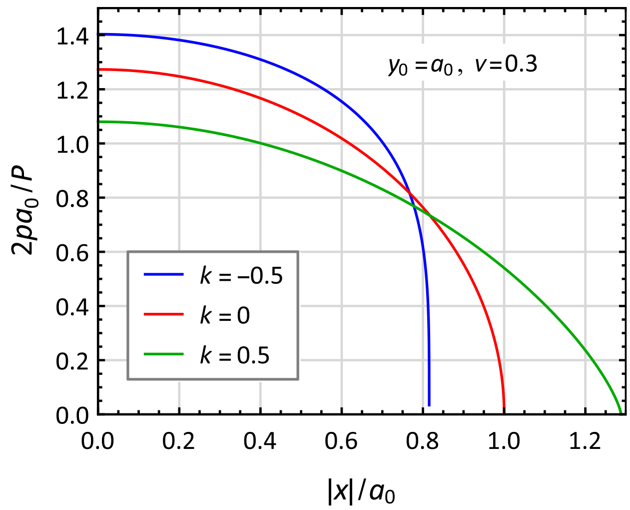

Fig. 7 Normalized pressure for selected values of the exponent of elastic inhomogeneity. The Poisson's ratio is v=0.3 and the characteristic depth is chosen to be equal to the contact half-width when indenting an elastically homogeneous half-plane

The position of the deformed surface of the half-plane outside the contact measured from the lowest point of indentation as well as the indentation depth must be determined from formulae (17) and (19). After the result from Eq. (33) has been inserted a short calculation leads to

$$h_y\left(x,a\right)=\frac{a^2}{Rk}\left[\frac{1}{2}-\frac{\sqrt{\pi}}{2\Gamma\left(\frac{4+k}{2}\right)\Gamma\left(\frac{1-k}{2}\right)}\left|\frac{a}{x}\right|^k {}_2F_1\left(\frac{k}{2},\frac{1+k}{2};\frac{4+k}{2};\frac{a^2}{x^2}\right)\right],\quad \left|x\right|\geq a\,, \tag{38}$$

and

$$\delta_y\left(a\right)=\frac{a^2}{2Rk},\quad 0<k<1\,. \tag{39}$$

4.2 Extension to Adhesive Solution

We now extend the normal contact problem to consider the effect of adhesive interaction within the contact region. Fig. 8 illustrates this kind of contact including its characteristic JKR-neck which resembles a mode I crack tip in linear elastic fracture mechanics.

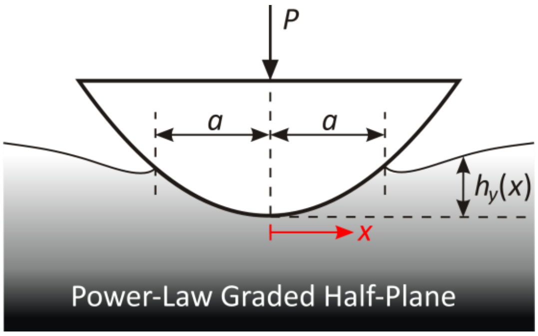

Fig. 8 Plane strain adhesive normal contact between a rigid parabolic cylinder with radius of curvature *R* and a power-law graded half-space

After substituting the solution of the non-adhesive normal contact given by Eq. (34) into Eq. (27), the line load as a function of the contact half-width is obtained

$$P\left(a\right)=\frac{\sqrt{\pi}E_0a^{k+2}}{2b\left(k,\nu\right)R\,y_0^k k\,\Gamma\left(\frac{4+k}{2}\right)\Gamma\left(\frac{1-k}{2}\right)}-\sqrt{\frac{4\Delta\gamma\sqrt{\pi}E_0a^{k+1}}{b\,k\,y_0^k\,\Gamma\left(\frac{2+k}{2}\right)\Gamma\left(\frac{1-k}{2}\right)}}\,. \tag{40}$$

Fig. 9 illustrates this relationship in normalized form for two different power-law graded half-planes. While a graded half-plane with k=0.1 is considered in Fig. 9(a), the curves for a grading with k=-0.1 are shown in Fig. 9(b). The curves on the left already indicate that the critical line load decreases in magnitude as the characteristic depth increases, while the critical contact half-width increases. For the PLG-half-plane characterized by k=-0.1, however, the opposite behavior occurs.

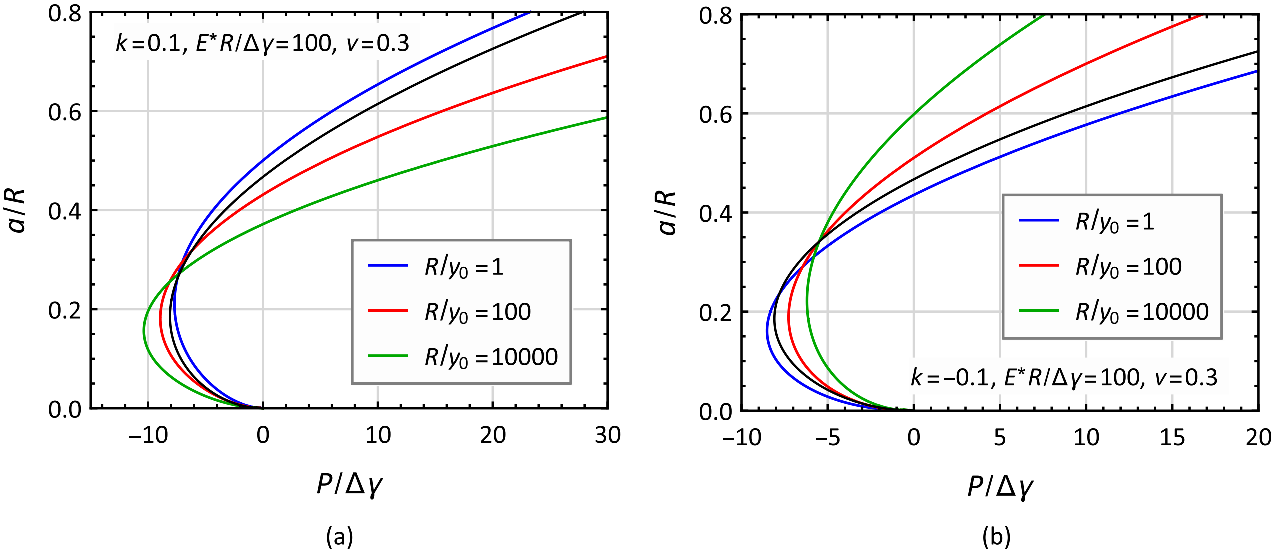

Fig. 9 Normalized relationship between contact half-width and line load for different characteristic depths and two representative in-depth gradings: (a) Positive in-depth grading with k = 0.1 and (b) Negative in-depth grading with k = -0.1. The Poisson's ratio was assumed to be ν = 0.3 and $E^*R/\Delta\gamma$ = 100. The black line indicates the solution of Barquins for homogeneous material.

It should be noted that Giannakopoulos and Pallot [23] already present a series of basic equations for solving the present adhesive contact problem in the appendix of their work. They used the classical approach of minimizing the total potential energy but did not provide any in-depth analyses. Based on the approaches of Giannakopoulos and Pallot, Chen et al. [24] analyze the problem in a numerical way. In their opinion "*simple closed-form solutions cannot be obtained easily. Numerical calculation must be carried out to analyze the interfacial adhesion behavior*." This claim is somewhat surprising, as the authors indeed recognize that the solution can be composed of two parts. However, they do not take advantage of the fact that the universal rigid body part must correspond exactly to the critical line load at which a flat punch adhesive contact loses its stability. This is the last term on the right-hand side in Eq. (27) or Eq. (40). Fig. 9(a) matches exactly the Fig. 4 from Chen *et al.* generated from numerical calculations.

The dependence of the contact half-width from the line load for different exponents of elastic inhomogeneities and two chosen characteristic depths is depicted in Fig. 10. For the curves on the left, Fig. 10(a), the characteristic depth was chosen to be equal to the radius of curvature of the parabolic cylinder. In this case, the maximum pull-off force decreases as the exponent of the elastic inhomogeneity increases, while the critical contact half-widths become larger. In Fig. 10(b), a 100 times smaller characteristic depth was set (y_0=R/100). For this specification, the maximum pull-off line load increases with increasing exponent of the elastic inhomogeneity, while the critical contact half-widths remain approximately the same. Note, that these results are qualitatively consistent with the findings of Li and Liu [25] (for high Tabor parameter), who study the adhesive plane strain contact problem between a graded coated half-space and a cylindrical indenter by using a Maugis model. The influence of the FGM coating thickness can be roughly understood as the influence of the characteristic depth. A stiffness ratio of the FGM coating (ratio of Young's moduli at its top and bottom) greater than 1 can be roughly interpreted as a negative exponent of elastic inhomogeneity, whereas a positive one represents stiffness ratios lower than 1.

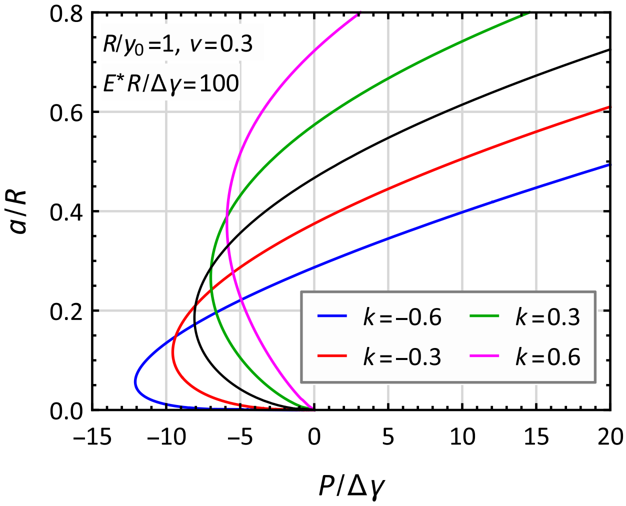

(a)

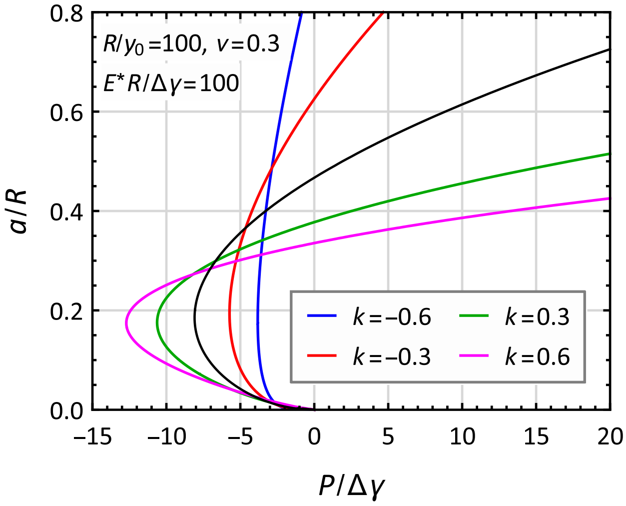

(b)

Fig. 10 Normalized relationship between contact half-width and line load for different exponents of elastic inhomogeneities and two representative characteristic depths: (a) Characteristic depth y_0 is equal to radius of curvature (b) Characteristic depth y_0 is significant smaller than radius of curvature. The Poisson's ratio was assumed to be ν = 0.3 and $E^*R/\Delta\gamma$ = 100. The black line indicates the solution of Barquins for homogeneous material.

The critical half-width, at which the contact loses its stability and detaches spontaneously, results from condition (31),

$$a_c = \left(\frac{k(k+1)^2 \Gamma\left(\frac{2+k}{2}\right)\Gamma\left(\frac{1-k}{2}\right) b\Delta\gamma y_0^k R^2}{\sqrt{\pi} E_0} \right)^{\frac{1}{3+k}}, \tag{41}$$

and the corresponding critical line load is

$$P_c = -\frac{(k+1)(k+3)\Delta\gamma R}{k+2} \left(\frac{\sqrt{\pi} E_0}{k(k+1)^2 \Gamma\left(\frac{2+k}{2}\right)\Gamma\left(\frac{1-k}{2}\right) b\Delta\gamma y_0^k R^2} \right)^{\frac{1}{3+k}}. \tag{42}$$

Taking $\lim_{k\to 0}\left[kb(k,\nu)\right] = 2\left(1-\nu^2\right)/\pi$ into account, the limit k → 0 of Eqs. (40) to (42) yield the known results for elastically homogeneous material originating from Barquins [26]

$$P(a) = \frac{\pi E^* a^2}{4R} - \sqrt{2\pi a E^* \Delta\gamma}, \quad a_{c,\text{JKR}} = \left(\frac{2R^2\Delta\gamma}{\pi E^*}\right)^{1/3}, \quad P_{c,\text{JKR}} = -3\left(\frac{\pi\Delta\gamma^2 R E^*}{16}\right)^{1/3}, \tag{43}$$

where $E^* = E_0/(1-\nu^2)$. The thin black lines in Fig. 9 and Fig. 10 represent the corresponding curve of the contact half-width as a function of the line load.

Using the critical values given in Eq. (43) for homogeneous elastic material for normalization, Fig. 11 clarifies the effect of the exponent of elastic inhomogeneity and the characteristic depth on the critical contact half-width and the critical line load (pull-off force per unit length). It becomes evident that both have a significant influence on the critical values. For the largest characteristic depths y_0, the critical half-width increases monotonically with rising k where the half-width for negative k being smaller and for positive ones larger than that for homogeneous elastic material. For moderate characteristic depths, there are no substantial deviations from the half-width for homogeneous material over a wide range of exponents of elastic inhomogeneity (-0.7<*k*<0.9). For the smallest characteristic depth y_0 considered, an interesting curve emerges with a pronounced relative maximum around 3.68 at *k*≈-0.78 and a relative minimum around 0.384 at *k*≈0.83 (green curve in Fig. Fig. 11(a)). The maximum pull-off force (per unit length) depicted in Fig. 11(b) exhibits a monotonically decreasing behavior with increasing exponent for the largest characteristic depth considered. For smaller characteristic depths, the maximum line load for negative *k* is smaller than that for homogeneous material and a monotonically increasing function in this range. The positive slope ends in a relative maximum in the range of positive exponents *k* and then goes steeply towards zero. The maximum in the case of y_0=0.0001R is located at *k*≈0.87 and amounts 4.34, i.e. the maximum pull-off line load is more than four times greater than that for homogeneous material.

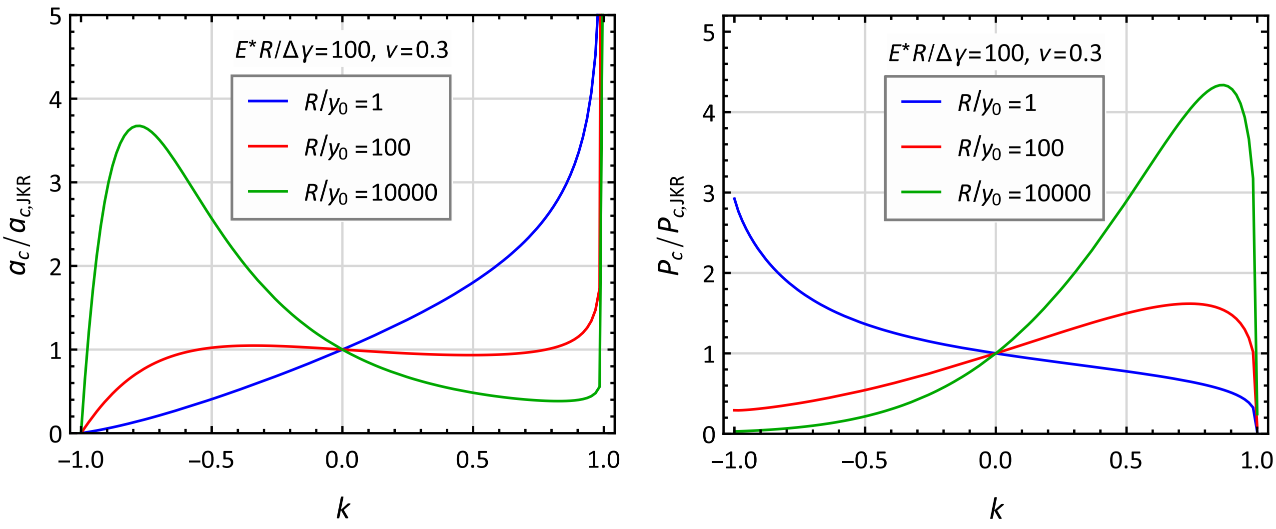

(a) (b)

Fig. 11 Effect of the exponent of the elastic inhomogeneity on (a) the critical contact half-width a_c and (b) the pull-off line load P_c. The Poisson's ratio was assumed to be ν = 0.3 and E*R/Δγ = 100.

Finally, the pressure distribution, the position of the deformed half-plane surface, and the indentation depth should be determined. For this purpose, the non-adhesive solutions (37) to (39) have to be inserted into Eqs. (28) to (30). The results are

$$p(x,a)=\frac{E_0 a^{k+1}}{2\Gamma\left(\frac{3+k}{2}\right)\Gamma\left(\frac{1-k}{2}\right)k\,b\,R\,y_0^k}\left(1-\frac{x^2}{a^2}\right)^{\frac{1+k}{2}}-\sqrt{\frac{4\Gamma\left(\frac{2+k}{2}\right)\Delta\gamma E_0 a^{k-1}}{\sqrt{\pi}\,b\,k\,y_0^k\,\Gamma\left(\frac{1+k}{2}\right)^2\Gamma\left(\frac{1-k}{2}\right)}}\left(1-\frac{x^2}{a^2}\right)^{\frac{k-1}{2}}, \quad (44)$$

$$\begin{aligned}h_y(x,a)=&\frac{a^2}{Rk}\left[\frac{1}{2}-\frac{\sqrt{\pi}}{2\Gamma\left(\frac{4+k}{2}\right)\Gamma\left(\frac{1-k}{2}\right)}\left|\frac{a}{x}\right|^k {}_2F_1\left(\frac{k}{2},\frac{1+k}{2};\frac{4+k}{2};\frac{a^2}{x^2}\right)\right]\\&-\sqrt{\frac{4by_0^k\Delta\gamma\sqrt{\pi}a^{1-k}}{E_0k\Gamma\left(\frac{2+k}{2}\right)\Gamma\left(\frac{1-k}{2}\right)}}\left[\frac{\Gamma\left(\frac{2+k}{2}\right)\Gamma\left(\frac{1-k}{2}\right)}{\sqrt{\pi}}-\left|\frac{a}{x}\right|^k {}_2F_1\left(\frac{k}{2},\frac{1+k}{2};\frac{2+k}{2};\frac{a^2}{x^2}\right)\right], \quad |x|\ge a\end{aligned}, \quad (45)$$

$$\delta_y(a)=\frac{a^2}{2Rk}-\sqrt{\frac{4\Gamma\left(\frac{2+k}{2}\right)\Gamma\left(\frac{1-k}{2}\right)\Delta\gamma b y_0^k a^{1-k}}{\sqrt{\pi}\,kE_0}}, \quad 0<k<1. \quad (46)$$

4.3 Adhesive Contact with Both Normal and Tangential Load

Chen *et al.* [24] also investigated the influence of a subsequently applied tangential load on the adhesive behavior. They made use of the common assumption that the application of the tangential load results in a constant tangential displacement of the contact region as a whole. In addition, they still assumed uncoupling of normal and tangential effects, i.e. normal stresses do not result in relative tangential displacements and vice versa. The authors once again solved this problem numerically, since they believe that closed-form analytical solutions are difficult to achieve, like in the case of pure normal loading. However, explicit analytical solutions can also be found in this case. This is possible by application of the recently introduced extension of Shull's compliance method by Heß and Forsbach [27] (see Eq. (29)). In this case, the elastic energy release rate according to Eq. (26) must be complemented by energetic contributions due to the tangential loading. For plane strain symmetric contact problems of half-width a, the following formulation has to be applied

$$G=\frac{\left(P_{\text{n.a.}}-P\right)^2}{4{S_y}^2}\frac{\mathrm{d}S_y}{\mathrm{d}a}+\frac{Q^2}{4{S_x}^2}\frac{\mathrm{d}S_x}{\mathrm{d}a},\quad S_y:=\frac{\mathrm{d}P_{\text{n.a.}}}{\mathrm{d}\delta_{y,\text{n.a.}}},\quad S_x:=\frac{\mathrm{d}Q_{\text{n.a.}}}{\mathrm{d}\delta_{x,\text{n.a.}}}, \tag{47}$$

where Q denotes the tangential line load and S_x the tangential contact stiffness. It should be emphasized that this condition can also be derived from the relationship between the energy release rate and the stress intensity factors at the edge of an adhesive tangential contact. It was probably first proposed by Johnson [28]. An equivalent approach in the framework of the method of dimensionality reduction was developed by Popov *et al.* [29]. They applied it to study the effect of a tangential displacement on the adhesion strength of a contact between a parabolic Indenter and an elastic half-space.

5. Conclusions

Based on the Mossakovskii-Jäger procedure, new formulae have been developed that allow closed-form analytical solutions of plane strain normal contacts between power-law graded elastic solids. By means of Shull's compliance method, these formulae were extended in a simple way to take JKR-adhesion into account. For this purpose, only the critical line load must be added, at which a flat punch in adhesive contact with a power-law graded half-plane loses its stability. To demonstrate the power of the new calculation tool, the adhesive plane strain contact of a cylinder and a power-law graded half-space was investigated. Until now, this problem could only be solved numerically. In contrast, we provide simple closed-form analytic solutions which include the range of negative exponents of elastic inhomogeneity and thus a negative in-depth grading. The results confirm that the critical contact half-width and the pull-off line load respond extremely sensitive to changes in the exponent of the elastic inhomogeneity, especially for small and large characteristic depths. For the smallest characteristic depth considered, the maximum of the critical half-width lies at $k\approx-0.78$ and is more than three times the critical half-width for homogeneous material. The pull-off line load on the other hand, has its maximum at $k\approx0.87$ and is more than four times higher than the classic value for homogeneous material.

The additional influence of a tangential line load can be investigated by means of an extension of Shull's compliance method presented in Sect. 4.3. Furthermore, due to the form analogy of the uncoupled integral equations (7), corresponding formulae for solving tangential contacts can be listed directly. In a follow-up work, these equations are used to study the effect of elastic grading on the local slip and the dissipated energy per loading cycle for plane strain fretting contacts. Studies for axisymmetric contacts have recently been conducted in collaboration with one of the authors [30].

Author Contributions

Conceptualization, M.H.; methodology, M.H. and P.G.; software, M.H. and P.G.; validation, M.H. and P.G.; formal analysis, M.H. and P.G.; investigation, M.H. and P.G.; writing—original draft preparation, M.H. and P.G.; writing—review and editing, M.H. and P.G.; visualization, M.H. and P.G.; supervision, M.H. All authors have read and agreed to the published version of the manuscript.

Funding

This research received no external funding.

Data Availability Statement

The data that support the findings of this study are available on request from the corresponding author.

Conflicts of Interest

The authors declare that they have no known competing financial interests or personal relationships that could have appeared to influence the work reported in this paper.

Acknowledgement

This research was not funded by any grant.

References

[1] Li, Y., Feng, Z., Hao, L., Huang, L., Xin, C., Wang, Y., Bilotti, E., Essa, K., Zhang, H., Li, Z., Yan, F., & Peijs, T. (2020). A review on functionally graded materials and structures via additive manufacturing: from multi-scale design to versatile functional properties. Advanced Materials Technologies, 5(6), 1900981. https://doi.org/10.1002/admt.201900981.

[2] Xiong, Y. Z., Gao, R. N., Zhang, H., Dong, L. L., Li, J. T., & Li, X. (2020). Rationally designed functionally graded porous Ti6Al4V scaffolds with high strength and toughness built via selective laser melting for load-bearing orthopedic applications. Journal of the mechanical behavior of biomedical materials, 104, 103673. https://doi.org/10.1016/j.jmbbm.2020.103673.

[3] Hou, C., Liu, Y., Xu, W., Lu, X., Guo, L., Liu, Y., Tian, S., Liu, B., Zhang, J., & Wen, C. (2022). Additive manufacturing of functionally graded porous titanium scaffolds for dental applications. Biomaterials Advances, 139, 213018. https://doi.org/10.1016/j.bioadv.2022.213018.

[4] Johnson, K. L. (1985). Contact mechanics. Cambridge University Press. Cambridge.

[5] Barber, J. R. (2018). Contact mechanics. Springer. https://doi.org/10.1007/978-3-319-70939-0.

[6] Popov, V. L., Heß, M., & Willert, E. (2019). Handbook of contact mechanics: exact solutions of axisymmetric contact problems. Springer Nature. https://doi.org/10.1007/978-3-662-58709-6.

[7] Popov, G. I. (1973). Plane contact problem for a linearly deformation foundation in the presence of adhesion. Journal of Applied Mathematics and Mechanics, 37(2), 254-261. https://doi.org/10.1016/0021-8928(73)90032-4.

[8] Antipov, Y. A., & Mkhitaryan, S. M. (2023). Hertzian and adhesive plane models of contact of two inhomogeneous elastic bodies. European Journal of Applied Mathematics, 34(4), 667-700. https://doi.org/10.1017/S0956792522000237.

[9] Argatov, I. (2019). On the size effects in indentation testing of elastic functionally-graded materials. New Achievements in Continuum Mechanics and Thermodynamics: A Tribute to Wolfgang H. Müller, 17-28. https://doi.org/10.1007/978-3-030-13307-8_2.

[10] Mossakovskii, V. I. (1963). Compression of elastic bodies under conditions of adhesion (axisymmetric case). Journal of Applied Mathematics and Mechanics, 27(3), 630-643. https://doi.org/10.1016/0021-8928(63)90150-3.

[11] Jäger, J. (1997). Half-planes without coupling under contact loading. Archive of applied mechanics, 67, 247-259. https://doi.org/10.1007/s004190050115.

[12] Jäger, J. (1998). A new principle in contact mechanics. Journal of tribology, 120(4), 677-684. https://doi.org/10.1115/1.2833765.

[13] Jäger, J. (2002). New analytical and numerical results for two-dimensional contact profiles. International journal of solids and structures, 39(4), 959-972. https://doi.org/10.1016/S0020-7683(01)00198-6.
[14] Heß, M. (2023). Some remarks on the two-dimensional contact of dissimilar elastic solids under non-slipping boundary conditions. Reports in Mechanical Engineering, 4(1), 290-309. https://doi.org/10.31181/rme040129112023h.
[15] Jin, F., & Guo, X. (2013). Mechanics of axisymmetric adhesive contact of rough surfaces involving power-law graded materials. International Journal of Solids and Structures, 50(20-21), 3375-3386. https://doi.org/10.1016/j.ijsolstr.2013.06.007.
[16] Heß, M., & Li, Q. (2023). Tangential contacts of three-dimensional power-law graded elastic solids: A general theory and application to partial slip. Mechanics of Advanced Materials and Structures, 1-21. https://doi.org/10.1080/15376494.2023.2222289.
[17] Booker, J. R., Balaam, N. P., & Davis, E. H. (1985). The behaviour of an elastic non-homogeneous half-space. Part II–circular and strip footings. International Journal for Numerical and Analytical Methods in Geomechanics, 9(4), 369-381. https://doi.org/10.1002/nag.1610090406.
[18] Hills, D., Sackfield, A., & Paynter, R. H. (2009). Simulation of Fretting Wear in Halfplane Geometries: Part 1—The Solution for Long Term Wear. Journal of tribology, 131(3), 031401. https://doi.org/10.1115/1.3118785.
[19] Popov, V. L. (2014). Analytic solution for the limiting shape of profiles due to fretting wear. Scientific reports, 4(1), 3749. https://doi.org/10.1038/srep03749.
[20] Heß, M. (2019). A study on gross slip and fretting wear of contacts involving a power-law graded elastic half-space. Facta Universitatis, Series: Mechanical Engineering, 17(1), 47-64. https://doi.org/10.22190/FUME190121010H.
[21] Shull, K. R., Ahn, D., Chen, W. L., Flanigan, C. M., & Crosby, A. J. (1998). Axisymmetric adhesion tests of soft materials. Macromolecular Chemistry and Physics, 199(4), 489-511. https://doi.org/10.1002/(SICI)1521-3935(19980401)199:4%3C489::AID-MACP489%3E3.0.CO;2-A
[22] Shull, K. R. (2002). Contact mechanics and the adhesion of soft solids. Materials Science and Engineering: R: Reports, 36(1), 1-45. https://doi.org/10.1016/S0927-796X(01)00039-0.
[23] Giannakopoulos, A. E., & Pallot, P. (2000). Two-dimensional contact analysis of elastic graded materials. Journal of the Mechanics and Physics of Solids, 48(8), 1597-1631. https://doi.org/10.1016/S0022-5096(99)00068-X.
[24] Chen, S., Yan, C., & Soh, A. (2009). Adhesive behavior of two-dimensional power-law graded materials. International Journal of Solids and Structures, 46(18-19), 3398-3404. https://doi.org/10.1016/j.ijsolstr.2009.05.006.
[25] Li, P., & Liu, T. J. (2018). The adhesive contact problem between a graded coated half-space and a cylindrical indenter by using a Maugis model. Journal of Adhesion Science and Technology, 32(22), 2494-2508. https://doi.org/10.1080/01694243.2018.1483291.
[26] Barquins, M. (1988). Adherence and rolling kinetics of a rigid cylinder in contact with a natural rubber surface. The Journal of Adhesion, 26(1), 1-12. https://doi.org/10.1080/00218468808071271.
[27] Heß, M., & Forsbach, F. (2020). Macroscopic modeling of fingerpad friction under electroadhesion: Possibilities and limitations. Frontiers in Mechanical Engineering, 6, 567386. https://doi.org/10.3389/fmech.2020.567386.
[28] Johnson, K. L. (1997). Adhesion and friction between a smooth elastic spherical asperity and a plane surface. Proceedings of the Royal Society of London. Series A: Mathematical, Physical and Engineering Sciences, 453(1956), 163-179. https://doi.org/10.1098/rspa.1997.0010.
[29] Popov, V. L., Lyashenko, I. A., & Filippov, A. E. (2017). Influence of tangential displacement on the adhesion strength of a contact between a parabolic profile and an elastic half-space. Royal Society Open Science, 4(8), 161010. https://doi.org/10.1098/rsos.161010.
[30] Wilhayn, J., & Heß, M. (2022). Frictional Energy Dissipation in Partial Slip Contacts of Axisymmetric Power-Law Graded Elastic Solids under Oscillating Tangential Loads: Effect of the Geometry and the In-Depth Grading. Mathematics, 10(19), 3641. https://doi.org/10.3390/math10193641.